Mind the Resonances: Final stages of accretion into bumpy black holes

Georgios Lukes-Gerakopoulos[1] and George Contopoulos[2]

[1] Theoretical Physics Institute, University of Jena,
07743 Jena, Germany
[2] Research Center for Astronomy and Applied Mathematics, Academy of Athens,
Soranou Efesiou 4, GR-11527 Athens, Greece

E-mail: gglukes@gmail.com

Abstract. In this article we discuss a possible way of testing the Kerr black hole hypothesis by taking advantage of phenomena correlated with chaotic motion in the final stages of an accretion disk around a bumpy black hole. We anticipate that these phenomena should have an imprint in the electromagnetic spectrum coming from the accretion disk.

1. Introduction

The gravitational wave detectors are anticipated to provide observations which will help us to study massive compact objects and to test our theoretical expectations about their nature. Namely, the spacetime around black holes is expected to be described by the Kerr metric. One way to test the Kerr hypothesis is to search in the gravitational wave signals for any deviation from the corresponding signals we would expect to come from a Kerr spacetime background, see e.g., [1, 2, 3] and references therein. However, alternative tests for our expectation might be based on contemporary plausible astronomical observations. Namely, the Kerr hypothesis can be tested by studying the electromagnetic spectra coming from a black hole's surrounding environment (e.g., [4, 5, 6, 7, 8, 9, 10, 11]).

Both gravitational and electromagnetic Kerr hypothesis tests are usually applied on axially symmetric perturbations of the Kerr spacetime, such spacetimes are often called in the literature bumpy black holes (name given in [12]) or non-Kerr spacetimes. By perturbing the Kerr spacetime it seems that in general we destroy a generalized Noether symmetry (e.g., [13] and references therein) responsible for the existence of the Carter constant [14]. Even if there are attempts of finding higher order Killing tensors expressing this symmetry in specific bumpy black hole spacetimes ([15] and references therein), the numerical results show that chaos appears when we examine geodesic orbits in these spacetimes [16, 17, 18, 19, 20], which in turn implies that these spacetimes correspond to a non-integrable system and therefore no Carter-like constant can exist. On the other hand, if we demand the preservation of the Carter constant after the perturbation, it seems that we have to relax the requirement that the perturbed metric satisfies the Einstein equations [21]. Thus, it appears that after the perturbation of the Kerr metric we have to either lose the Carter constant or drop the requirement that the new metric has to satisfy the Einstein equations.

The non-integrability of the bumpy black holes is correlated with several interesting aspects of classical non-integrable systems. In particular, in [19] we have studied how the bifurcation of the periodic orbits at the resonances lead to escaping orbits in a classical system of two coupled harmonic oscillators and a relativistic system described by a subclass of the Manko-Novikov (MN) metric family [22]. In the present article we attempt to give a physical interpretation to the study done in [19]. Namely, we try to interpret our findings as possible imprints in the electromagnetic spectra indicating a method to distinguish bumpy black hole spacetimes from Kerr spacetimes by exploiting the non-linear phenomena studied in [19] at the final stages of accretion into a non-Kerr compact object, in a similar way as done by the authors of [23].

The article is organized as follows. We introduce the MN spacetime in section 2. Section 3 summarizes basic elements of geodesic motion in axisymmetric and stationary spacetimes. We discuss, by interpreting the numerical examples given in [19], the final stages of accreting matter into a MN bumpy black hole in section 4. Section 5 briefs our main conclusion.

2. The Manko-Novikov spacetime

The bumpy black hole spacetime we used in [19] is a spacetime which belongs to the so-called Manko-Novikov (MN) metric family [22]. Manko and Novikov found an exact vacuum solution of Einstein's equations which describes a stationary, axisymmetric, and asymptotically flat spacetime with arbitrary mass-multipole moments [22]. The MN metric subclass we used was introduced by [16] and deviates from the Kerr by the anomalous quadrupole moment q. The quantity q measures how much the MN quadrupole moment Q departs from the Kerr quadrupole moment $Q_{Kerr} = -S^2/M$ (i.e., $q = (Q_{Kerr} - Q)/M^3$), where M and S are the mass and spin of a Kerr black hole. The line element of the MN metric in the Weyl-Papapetrou cylindrical coordinates (ρ, φ, z) is

$$ds^2 = -f(dt - \omega d\varphi)^2 + f^{-1}[e^{2\gamma}(d\rho^2 + dz^2) + \rho^2 d\varphi^2], \tag{1}$$

where f, ω, γ are considered as functions of the prolate spheroidal coordinates v, w, while the coordinates ρ, z can be expressed as functions of v, w as well. Thus

$$\rho = k\sqrt{(v^2 - 1)(1 - w^2)}, \quad z = kvw, \tag{2}$$

and

$$f = e^{2\psi}\frac{A}{B}, \tag{3a}$$

$$\omega = 2ke^{-2\psi}\frac{C}{A} - 4k\frac{\alpha}{1 - \alpha^2}, \tag{3b}$$

$$e^{2\gamma} = e^{2\gamma'}\frac{A}{(v^2 - 1)(1 - \alpha^2)^2}, \tag{3c}$$

$$A = (v^2 - 1)(1 + a\,b)^2 - (1 - w^2)(b - a)^2, \tag{3d}$$

$$B = [(v + 1) + (v - 1)a\,b]^2 + [(1 + w)a + (1 - w)b]^2, \tag{3e}$$

$$C = (v^2 - 1)(1 + a\,b)[(b - a) - w(a + b)]$$
$$+ (1 - w^2)(b - a)[(1 + a\,b) + v(1 - a\,b)], \tag{3f}$$

$$\psi = \beta\frac{P_2}{R^3}, \tag{3g}$$

$$\gamma' = \ln\sqrt{\frac{v^2 - 1}{v^2 - w^2}} + \frac{3\beta^2}{2R^6}(P_3^2 - P_2^2)$$
$$+ \beta\left(-2 + \sum_{\ell=0}^{2}\frac{v - w + (-1)^{2-\ell}(v + w)}{R^{\ell+1}}P_\ell\right), \tag{3h}$$

$$a = -\alpha \exp\left[-2\beta\left(-1 + \sum_{\ell=0}^{2}\frac{(v-w)P_\ell}{R^{\ell+1}}\right)\right], \tag{4a}$$

$$b = \alpha \exp\left[2\beta\left(1 + \sum_{\ell=0}^{2}\frac{(-1)^{3-\ell}(v+w)P_\ell}{R^{\ell+1}}\right)\right], \tag{4b}$$

$$R = \sqrt{v^2 + w^2 - 1}, \tag{4c}$$

$$P_\ell = P_\ell(\frac{v\,w}{R}). \tag{4d}$$

Here $P_\ell(\zeta)$ is the Legendre polynomial of order l

$$P_\ell(\zeta) = \frac{1}{2^\ell \ell!}\left(\frac{d}{d\zeta}\right)^\ell (\zeta^2 - 1)^\ell, \tag{5}$$

while the parameters k, α, β are related to the mass M, the spin S, and the quadrupole deviation q through the expressions

$$\alpha = \frac{-1+\sqrt{1-\chi^2}}{\chi}, \quad k = M\frac{1-\alpha^2}{1+\alpha^2}, \quad \beta = q\left(\frac{1+\alpha^2}{1-\alpha^2}\right)^3. \tag{6}$$

while χ is the dimensionless spin parameter $\chi = S/M^2$. These formulae give the Kerr metric for $q = 0$. We use the geometrical units $c = G = 1$ throughout the article, and without loss of generality we have set also $M = 1$.

3. Geodesic Motion in the Manko-Novikov spacetime

The geodesic orbits of a test particle of mass μ are described as equations of motion of the following Lagrangian

$$L = \frac{1}{2}\,\mu\,g_{\mu\nu}\,\dot{x}^\mu \dot{x}^\nu, \tag{7}$$

where the dots mean derivatives with respect to the proper time. Except from the Lagrangian itself $L = -\mu$, the MN metric has two more integrals of motion, namely the energy (per unit mass)

$$E = -\frac{\partial L}{\partial \dot{t}}/\mu = f(\dot{t} - \omega\,\dot{\varphi}), \tag{8}$$

and the z-component of the angular momentum (per unit mass)

$$L_z = \frac{\partial L}{\partial \dot{\varphi}}/\mu = f\omega(\dot{t} - \omega\,\dot{\varphi}) + f^{-1}\rho^2\dot{\varphi}, \tag{9}$$

The Kerr metric has one more integral of motion which is independent and in involution with the other integrals, the so-called Carter constant [14]. Thus the Kerr metric corresponds to an integrable system. However, the MN model misses such a constant, which means that MN corresponds to a non-integrable system, and therefore chaos may appear.

By simple algebraic manipulations of the metric (1) and the eqs. (8), (9) we find that the MN system satisfies the relation

$$\frac{1}{2}(\dot{\rho}^2 + \dot{z}^2) + V_{\text{eff}}(\rho, z) = 0, \tag{10}$$

where the effective potential $V_{\text{eff}}(\rho, z)$ depends on q, E and L_z, and the geodesic motion can be restricted on a meridian plane ($\varphi = \text{const}$). Moreover, the motion takes place inside a region defined by $V_{\text{eff}}(\rho, z) \leq 0$, the border of which is the curve of zero velocity (CZV)

$$V_{\text{eff}} \equiv \frac{1}{2} e^{-2\gamma} \left[f - E^2 + \left(\frac{f}{\rho} (L_z - \omega E) \right)^2 \right] = 0. \tag{11}$$
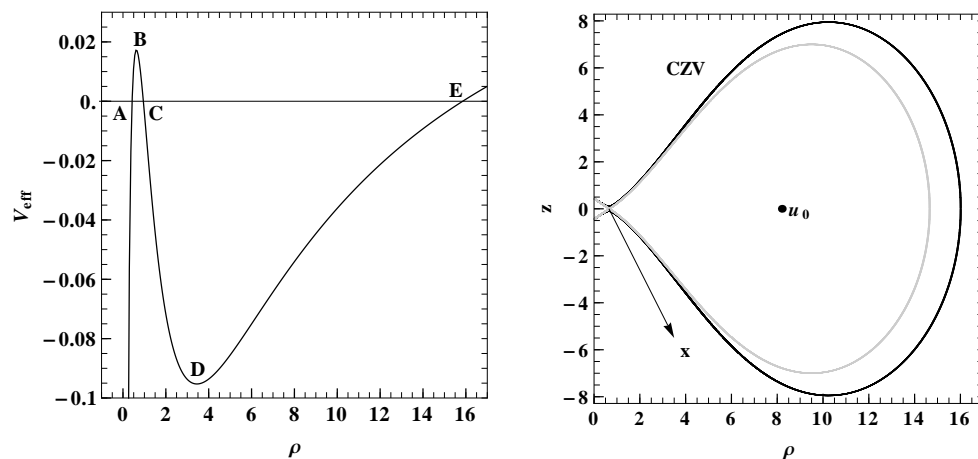
Figure 1. The left panel shows the portrait of the effective potential V_{eff} along the equatorial line ($z = 0$) for $E = 0.95$, $L_z = 2.5$, $\chi = 0.9$, and $q = 0$ (Kerr metric). The horizontal line $V_{\text{eff}} = 0$ indicates the upper limit reached by the non-escaping to infinity orbits, while the letters A, C, and E indicate the position of the roots of V_{eff}. Letters B, and D indicate the position of local extrema of V_{eff}. The right panel shows the CZV (black curve) on the meridian plane (ρ, z) for a slightly lower angular momentum than in the left panel ($L_z = 2.46$), the separatrix (gray curve) emanating from the unstable periodic orbit labeled by the letter "x" and the crossing of a stable periodic orbit through the $z = 0$ line (big dot) labeled by $\mathbf{u}_0$.

From the shape of the effective potential (11) we can discern the basic dynamics of the system like in a classical system. For instance in the integrable case of the Kerr metric the roots of the effective potential provide the boundaries of the non-escaping to infinity orbits (A, C, E in the left panel of Fig. 1). Between C and E lie the bounded non-plunging orbits, while from A leftwards lie the orbits that are plunging to the black hole (left panel of Fig. 1). Moreover, the local extrema of V_{eff} implies the existence of simple periodic orbits, for example the local minimum D indicates the existence of a simple stable periodic orbit indicated by $\mathbf{u}_0$ in the right panel of Fig. 1, while the local maximum B implies that a simple unstable periodic orbit will appear (x in the right panel of Fig. 1) for a specific range of V_{eff} parameters, namely if we lower the L_z in the case shown in the left panel of 1 to $L_z = 2.46$. When the local maximum B becomes negative, the separation between plunging and non-plunging orbits is defined by the separatrix (gray curve in the right panel) emanating from the unstable periodic orbit x. The orbits which lay between $\mathbf{u}_0$ and the part of the separatrix encircling $\mathbf{u}_0$ are bounded non-plunging orbits, all the other orbits inside the CZV plunge into the black hole. For a specific set of E and L_z values (lower than those in Fig. 1), when all the five points indicated by the letters shown in the left panel of Fig. 1 have merged into one point, the periodic orbits x and $\mathbf{u}_0$ merge into an indifferently stable periodic orbit, which is known in the bibliography as the Innermost Stable Circular Orbit (ISCO). Inside from an ISCO (leftwards in Fig. 1) only plunging orbits exist.
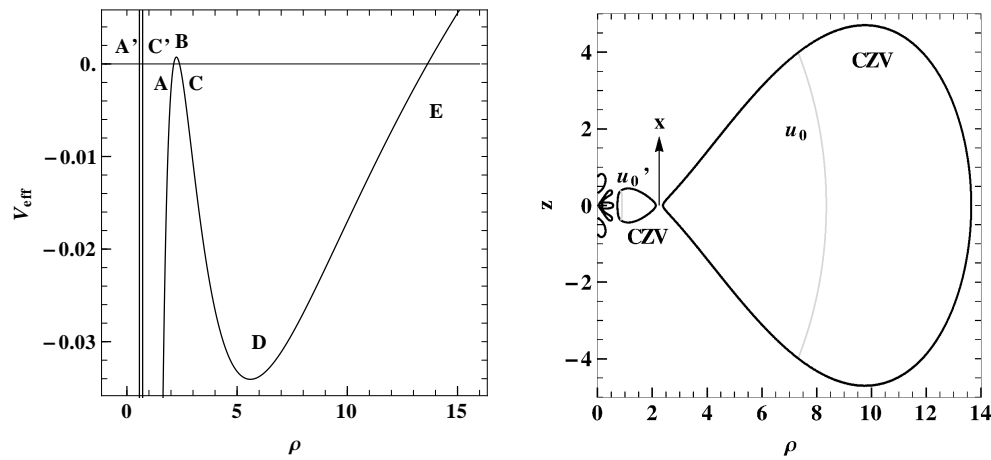
Figure 2. The left panel shows the portrait of the effective potential V_{eff} along the equatorial line ($z = 0$) for $E = 0.95$, $L_z = 3$, $\chi = 0.9$, and $q = 0.95$. The letters A′, C′, A, C and E indicate the position of the roots of V_{eff}. Letters B, and D indicate the position of local extrema of V_{eff}. The right panel shows the CZVs (black curves) on the meridian plane (ρ, z), and the projections on the plane of the simple stable periodic orbits $\mathbf{u}_0$, $\mathbf{u}_0'$ (gray curves). While x indicates the region where an unstable periodic orbit will appear for lower angular momentum L_z, or greater energy E.

In the case of the subclass of the MN family and for the parameters we have examined, the V_{eff} takes a little bit different shape (left panel of Fig. 2). Except from the roots we have seen in the Kerr case, two extra root appear the A′ and C′. Hence, an extra non-plunging region between C′ and A appear. The local minimum between C′ and A is extremely low (far out of the range shown in Fig. 2) and it indicates the existence of a new simple stable periodic orbit ($\mathbf{u}_0'$ in the right panel of Fig. 2). B and D again indicate a simple unstable periodic orbit (when B is below V_{eff}) and a simple stable periodic orbit (x and $\mathbf{u}_0$ in the right panel of Fig. 2) respectively. Similarly as in the Kerr case, for a specific set of E and L_z values, when all the five points indicated by the not primed letters shown in the left panel of Fig. 2 have merged into one point, the periodic orbits x and $\mathbf{u}_0$ merge into an indifferently stable periodic orbit, which although it is not the innermost stable circular orbit, we are going to call it ISCO, like the authors of [23] did. Moreover, five leaf-like plunging regions appear on the left side of the right panel of Fig. 2.

If we cut the phase space along the along the equatorial plane ($z = 0$) plane and keep only the orbits crossing it with positive velocity, we produce a surface of section, also known as a Poincaré section. In Fig. 3 we show such a section and the periodic orbits x, $\mathbf{u}_0'$ and $\mathbf{u}_0$ on it. The scattered points seen in Fig. 3 belong to a chaotic region. Because the MN corresponds to a non-integrable system, this chaotic region is swept densely by the asymptotic manifolds emanating from x instead of the separatrix of the integrable case.

4. The final stages of an accretion disk in a Manko-Novikov spacetime
Bambi and Barausse in [23] found that during the accretion process in MN spacetime the gas crossing the ISCO can follow four different types of plunge:

(i) The gas plunges radially into the compact object like in the Kerr case.

(ii) The gas plunges radially, but gets trapped in a region near the compact object.

(iii) The gas plunges to the central object due to a vertical to the equator instability.
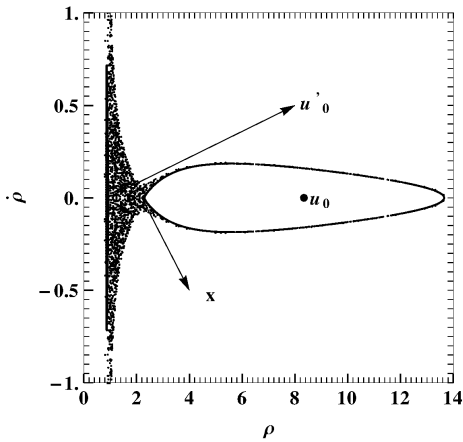
Figure 3. A Poincaré section $(\rho, \dot{\rho})$ along the $z = 0$ for $E = 0.95$, $L_z = 2.98$, $\chi = 0.9$, and $q = 0.95$. The position of the simple periodic orbit $\mathbf{u}_0$ is shown by a big dot, while the positions of the simple unstable periodic orbit x and of the simple periodic orbit $\mathbf{u}_0'$ are shown by arrows.

(iv) The gas plunges due to a vertical to the equator instability, but it gets trapped to two symmetrical to the equator regions.

Our study in a way follows up the second scenario, and explores what happens with the entrapped gas. The gas in our simple model consists of collisionless "test particle" fluid. We neglect the self-gravity of the gas, and the particles track the geodesic orbits of the MN spacetime background. The above approximation might seem a little irrelevant for a gas where the free path is short. However, when the gas particles collide, they just "exchange" their position in the phase space; in a great view they all still trace the background on which they are moving even if each of them individually does not follow geodesic orbit, but rather a great collection of small geodesic paths. In fact, we are not so interested on each particle's individual orbit, but rather we are concerned with the escape rate of a "swarm" of particles, thus, in our simple approximation we allow ourselves to ignore the collisions. Moreover, in our scenario the particles of the accretion matter share a constant angular momentum $L_z = 3$, but they radiate energy E away. This setup is like having a disk which radiates without losing its angular momentum.
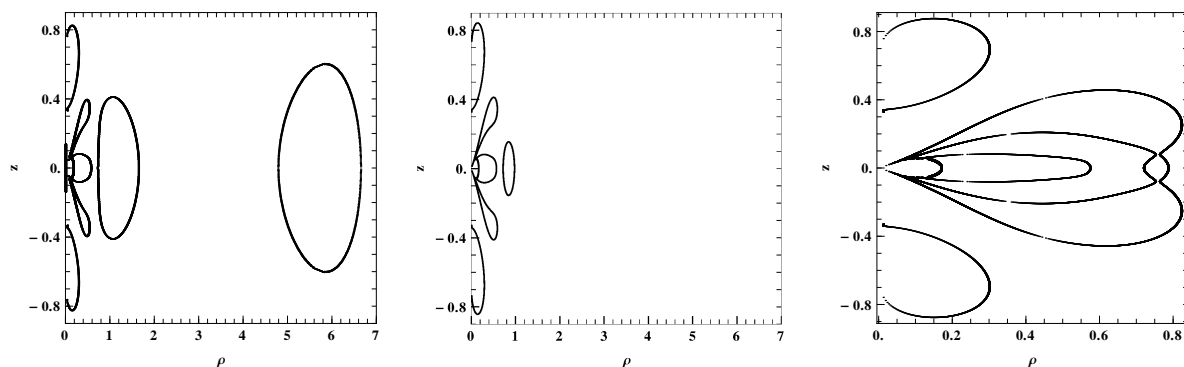
Figure 4. The CZVs as we reduce energy from the left panel to the right panel for constant $L_z = 3$ (beginning from left $E = 0.933$, $E = 0.7$, $E = 0.1899$).

We investigated the MN spacetime background for the values $q = 0.95$, and $\chi = 0.9$. By keeping the z-angular momentum $L_z = 3$ fixed and reducing the energy, the outer region around $\mathbf{u}_0$ (right panel of Fig. 2) gradually shrinks (left panel of Fig. 4), until it disappears and only the inner region around $\mathbf{u}_0'$ remains (central panel of Fig. 4). During the energy reduction the

leaf like plunging region on either side of the inner region expand rightwards towards the inner region, until they reach it (right panel of Fig. 4). Our study in [19] focuses on the phase space transition from having bounded non-plunging orbits to getting plunging orbits. One must keep in mind that all the different energy states coexist, and the particles slowly drift with different rates of energy loss towards the inner regions.
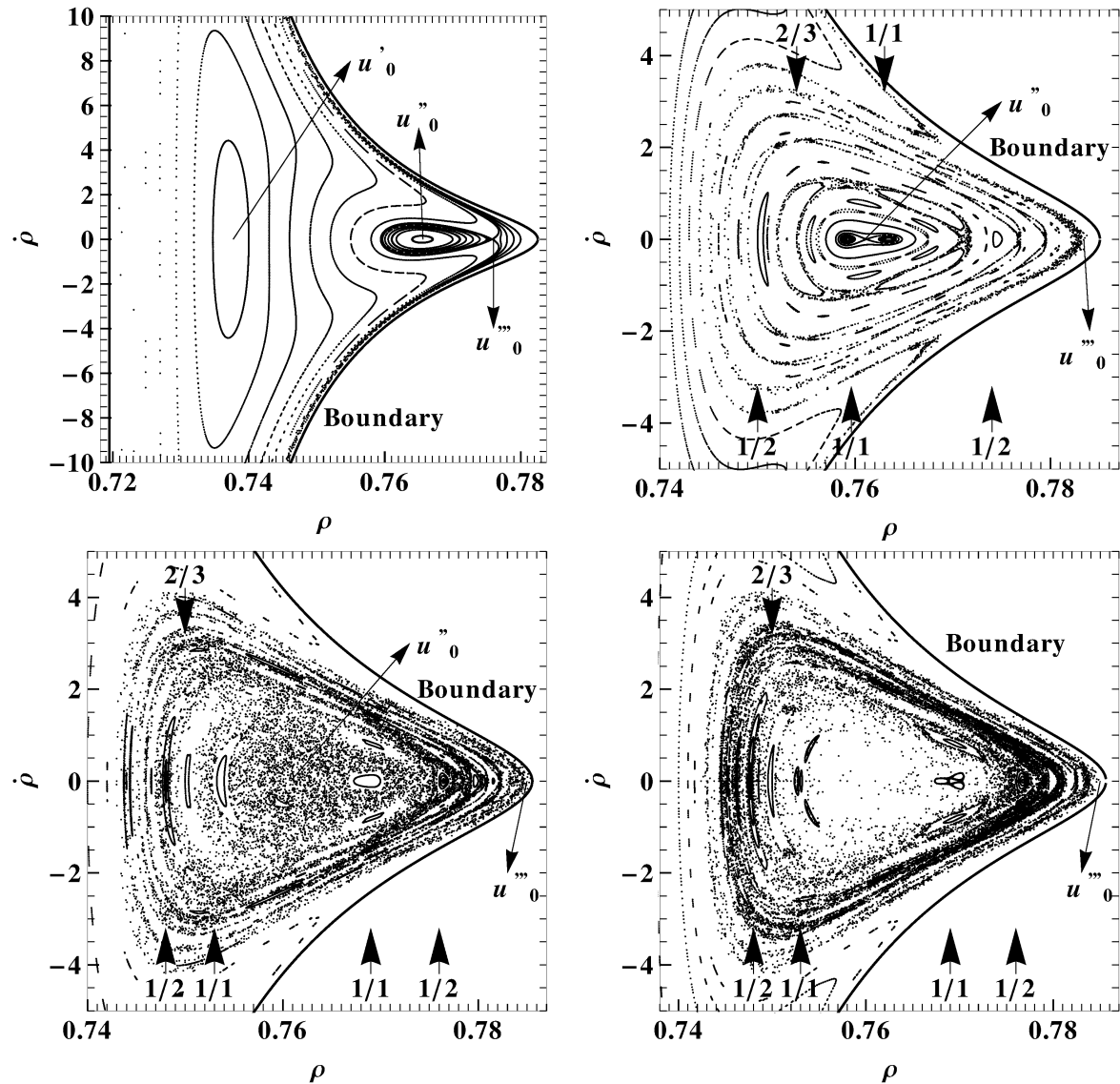
Figure 5. Surfaces of section $(\rho, \dot{\rho})$ for different energies: upper left panel $E = 0.192$, upper right panel $E = 0.19045$, lower left panel $E = 0.19015$ and lower right panel $E = 0.1901$. On the plots the simple periodic orbits $\mathbf{u}_0'$, $\mathbf{u}_0''$, $\mathbf{u}_0'''$ and the positions on the $\dot{\rho} = 0$ line of low order periodic orbits 1/1, 1/2, 2/3 are labeled.

It is quite interesting to monitor the phase space transition of the inner region from a region containing non-plunging orbits to a region with plunging orbits. Initially the region is occupied mostly by regular orbits, but about $E = 0.192$ a tangent bifurcation produces a couple of new simple periodic orbits $\mathbf{u}_0''$, $\mathbf{u}_0'''$ (upper left panel of Fig. 5), a stable and an unstable one

respectively. The periodic orbit $\mathbf{u}_0''$ changes its stability to instability and vice versa an infinite number of times, while periodic orbits, like the low order ones seen in the upper right panel of Fig. 5, further bifurcate from it. This leads to a gradually increasing volume occupied by chaotic orbits (lower left panel of Fig. 5), and when the CZV around the inner region is reached by the leaf-like plunging region (right panel of Fig. 4), then the chaotic orbits lying around $\mathbf{u}_0''$ become plunging (lower right panel of Fig. 5). As the energy drops the period of $\mathbf{u}_0''$ increases and tends to infinity. In fact it becomes actually infinite when the CZV of the inner region opens up (see [19]). In a way the orbit of $\mathbf{u}_0''$ "traces" the path to the chaotic orbits in order for them to plunge.
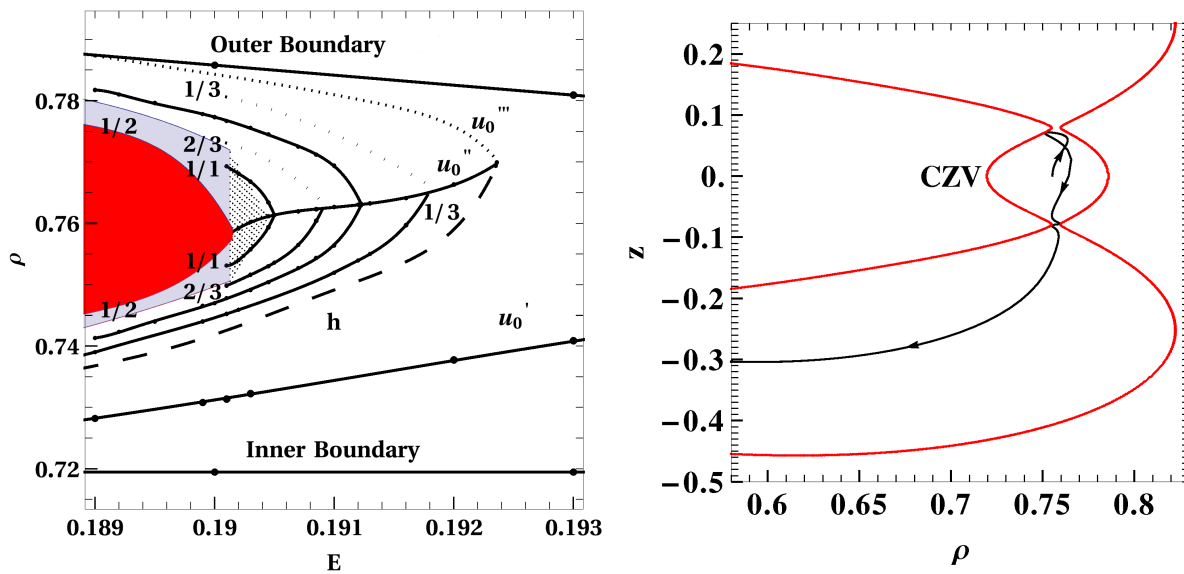
Figure 6. The left panel shows characteristics for the energy E of the families $\mathbf{u}_0'$, $\mathbf{u}_0''$, $\mathbf{u}_0'''$ and of some resonant bifurcations from the family $\mathbf{u}_0''$. The dotted region indicates regions where chaos is prominent. The gray region indicates regions with plunging orbits, while the red region gives the initial conditions (for $z = 0$) of orbits that plunge directly. The dashed line approximates the position of the first homoclinic section of the manifolds emanating from the orbit $\mathbf{u}_0'''$. The right panel shows a plunging orbit (black curve) and the CZV (red curve).

A summary of the procedure shown in Fig. 5 is given by the characteristic curves shown in the left panel of Fig. 6. This figure shows different bifurcations of the orbit $\mathbf{u}_0''$ and the creation of a prominent chaotic region (dotted region) around it as a function of the energy E, while E decreases. When the inner region joins the plunging region, the chaotic orbits become plunging (gray and red region). This mean that particles of our gas which move along a chaotic orbit will eventually plunge. Especially, particles moving along orbits corresponding to the red colored region (left panel of Fig. 6) will plunge directly, i.e., the particles will start from the equator but they will not cross it again with $\dot{z} > 0$ (e.g., in the right panel of Fig. 6 the orbit crosses the equator again but with $\dot{z} < 0$). The fact that the red region expands around the prolongation of the characteristic curve of the $\mathbf{u}_0''$ periodic orbit is in agreement with the aforementioned role of $\mathbf{u}_0''$ for creating a path for chaotic orbits to plunge, because it shows that the plunging paths lie around the $\mathbf{u}_0''$ periodic orbit. Thus, the left panel of Fig. 6 shows that the phase space undergoes an abrupt transition. Namely, the phase space ceases to be dominated by regular orbits and prominent chaotic regions appear just before the plunge begins.
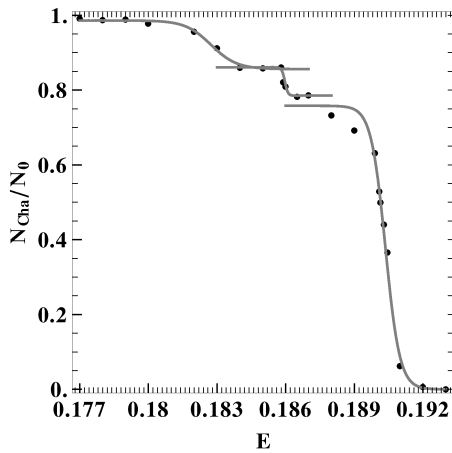
Figure 7. The proportion N_{cha}/N_0 of the chaotic-plunging orbits with initial conditions along the line $\dot{\rho} = 0$ as a function of the energy E.

This transition is shown better in Fig. 7, where we plot the proportion of chaotic-plunging orbits whose initial condition lie along the line $\dot{\rho} = 0$. The proportion changes abruptly at a narrow interval of decreasing energy values, and this implies that according to our simplistic model the majority of the gas particles will plunge along a non-equatorial trajectory, while their energy lies in this relatively narrow interval. Thus, in a electromagnetic spectrum coming from the vicinity of the MN central compact body we would expect a characteristic imprint of such a plunge, because the plunging particles are creating a non-radial cataclysmic inflow from the accretion disk. Moreover, in Fig. 7 we can see two more minor abrupt changes in the proportion N_{cha}/N_0, which means that we may have even some minor inflows as well, which will have their own characteristic imprints in the spectrum.

Since the particles move outside the equator our simplistic model should hold only when the enthalpy of the gas is small in comparison to the gravitational field of the central object. Otherwise, we have to take into account the gradient of the pressure of the gas and the geodesic approach has to be further investigated for its validity. On the other hand, we speculate that adding pressure would be just like putting a lid over a boiling pot, thus what we expect is that the energy interval of the cataclysmic inflow would just become narrower and the abrupt change in the fraction of chaotic plunging orbits (Fig. 7) more steep. Such a cataclysmic inflow of plunging matter should have an imprint on the radiation coming from the surrounding of the central compact object and could, in principle, be used as a method of detecting whether the black holes are described indeed by the Kerr metric or not, since such inflows are not expected to exist in the Kerr case.

5. Conclusions

By attempting to give an astrophysical interpretation to a dynamical study [19], we suggest a way that a cataclysmic inflow from an initially non-plunging region of the accreting matter towards the central compact object may lead to a method of testing the Kerr hypothesis by checking the electromagnetic spectra coming from the vicinity of the central compact object.

Acknowledgments

References

[1] Amaro-Seoane P, Aoudia S, Babak S and et al 2012 *Classical Quant. Grav.* **29** 124016 (*Preprint* gr-qc/1202.0839)

[2] Bambi C 2011 *Mod. Phys. Lett. A* **26** 2453–2468 (*Preprint* `gr-qc/1109.4256`)

[3] Johannsen T 2012 *Adv. Astron.* **2012** 486750 (*Preprint* `astro-ph.HE/1105.5645`)

[4] Bambi C 2012 *Phys. Rev. D* **85** 043002 (*Preprint* `gr-qc/1201.1638`)

[5] Bambi C 2012 *J. Cosmol. Astropart. Phys.* **9** 14 (*Preprint* `gr-qc/1205.6348`)

[6] Johannsen T and Psaltis D 2010 *Astrophys. J.* **716** 187–197 (*Preprint* `astro-ph.HE/1003.3415`)

[7] Johannsen T and Psaltis D 2010 *Astrophys. J.* **718** 446–454 (*Preprint* `astro-ph.HE/1005.1931`)

[8] Johannsen T and Psaltis D 2011 *Astrophys. J.* **726** 11 (*Preprint* `astro-ph.HE/1010.1000`)

[9] Johannsen T and Psaltis D 2011 *Adv. Space Res.* **47** 528–532 (*Preprint* `astro-ph.HE/1008.3902`)

[10] Johannsen T and Psaltis D 2012 (*Preprint* `astro-ph.HE/1202.6069`)

[11] Pappas G 2012 *Mon. Not. R. Astron. Soc.* **422** 2581–2589 (*Preprint* `astro-ph.HE/1201.6071`)

[12] Collins N A and Hughes S A 2004 *Phys. Rev. D* **69** 124022 (*Preprint* `gr-qc/0402063`)

[13] Markakis C (*Preprint* `astro-ph.SR/1202.5228`)

[14] Carter B 1968 *Phys. Rev.* **174** 1559–1571

[15] Brink J 2011 *Phys. Rev. D* **84** 104015 (*Preprint* `gr-qc/0911.4161`)

[16] Gair J R, Li C and Mandel I 2008 *Phys. Rev. D* **77** 024035 (*Preprint* `gr-qc/0708.0628`)

[17] Lukes-Gerakopoulos G, Apostolatos T A and Contopoulos G 2010 *Phys. Rev. D* **81** 124005 (*Preprint* `gr-qc/1003.3120`)

[18] Contopoulos G, Lukes-Gerakopoulos G and Apostolatos T A 2011 *Int. J. Bifurcat. Chaos* **21** 2261 (*Preprint* `gr-qc/1108.5057`)

[19] Contopoulos G, Harsoula M and Lukes-Gerakopoulos G 2012 *Celest. Mech. Dyn. Astron.* **113** 255–278 (*Preprint* `nlin.CD/1203.1010`)

[20] Lukes-Gerakopoulos G 2012 *Phys. Rev. D* **86** 044013 (*Preprint* `gr-qc/1206.0660`)

[21] Vigeland S, Yunes N and Stein L C 2011 *Phys. Rev. D* **83** 104027 (*Preprint* `gr-qc/1102.3706`)

[22] Manko V S and Novikov I D 1992 *Classical Quant. Grav.* **9** 2477–2487

[23] Bambi C and Barausse E 2011 *Phys. Rev. D* **84** 084034 (*Preprint* `gr-qc/1108.4740`)